1521-0111/94/6/1352–1362$35.00
MOLECULAR PHARMACOLOGY

https://doi.org/10.1124/mol.118.113142
Mol Pharmacol 94:1352–1362, December 2018

Activated CaMKIIα Binds to the mGlu$_5$ Metabotropic Glutamate Receptor and Modulates Calcium Mobilization[S]

Christian R. Marks, Brian C. Shonesy, Xiaohan Wang, Jason R. Stephenson, Colleen M. Niswender, and Roger J. Colbran

Departments of Molecular Physiology and Biophysics (C.R.M., B.C.S., J.R.S., R.J.C.) and Pharmacology (C.M.N.), Vanderbilt Brain Institute (X.W., R.J.C.), Vanderbilt Kennedy Center for Research on Human Development (C.M.N., R.J.C.), and Vanderbilt Center for Neuroscience Drug Discovery (C.M.N.), Vanderbilt University School of Medicine, Nashville, Tennessee

Received May 29, 2018; accepted September 19, 2018

ABSTRACT

Ca^{2+}/calmodulin-dependent protein kinase II (CaMKII) and metabotropic glutamate receptor 5 (mGlu$_5$) are critical signaling molecules in synaptic plasticity and learning/memory. Here, we demonstrate that mGlu$_5$ is present in CaMKIIα complexes isolated from mouse forebrain. Further in vitro characterization showed that the membrane-proximal region of the C-terminal domain (CTD) of mGlu$_{5a}$ directly interacts with purified Thr286-autophosphorylated (activated) CaMKIIα. However, the binding of CaMKIIα to this CTD fragment is reduced by the addition of excess Ca^{2+}/calmodulin or by additional CaMKIIα autophosphorylation at non-Thr286 sites. Furthermore, in vitro binding of CaMKIIα is dependent on a tribasic residue motif Lys-Arg-Arg (KRR) at residues 866–868 of the mGlu$_{5a}$-CTD, and mutation of this motif decreases the coimmunoprecipitation of CaMKIIα with full-length mGlu$_{5a}$ expressed in heterologous cells by about 50%. The KRR motif is required for two novel functional effects of coexpressing constitutively active CaMKIIα with mGlu$_{5a}$ in heterologous cells. First, cell-surface biotinylation studies showed that CaMKIIα increases the surface expression of mGlu$_{5a}$. Second, using Ca^{2+} fluorimetry and single-cell Ca^{2+} imaging, we found that CaMKIIα reduces the initial peak of mGlu$_{5a}$-mediated Ca^{2+} mobilization by about 25% while doubling the relative duration of the Ca^{2+} signal. These findings provide new insights into the physical and functional coupling of these key regulators of postsynaptic signaling.

Introduction

The ability of excitatory glutamatergic synapses to undergo dynamic changes in strength, termed synaptic plasticity, is critical for many behaviors. It is well established that glutamate activation of diverse ionotropic and metabotropic receptors is critical for short-term and long-term control of many neuronal responses (Niswender and Conn, 2010), and that these responses require a complex and incompletely understood network of signaling proteins. Among the seven members of the metabotropic glutamate (mGlu) receptor family, mGlu$_1$ and mGlu$_5$ specifically couple through G$\alpha_{q/11}$ to stimulate multiple signaling pathways, including phosphoinositide hydrolysis and mobilization of intracellular Ca^{2+} stores. These receptors have long been implicated in multiple forms of long-term depression that require new protein synthesis (Oliet et al., 1997; Palmer et al., 1997; Huber et al., 2001) or increased endocannabinoid signaling (Lüscher and Huber, 2010). Despite many similarities, mGlu$_1$ and mGlu$_5$ can be differentially regulated by various mechanisms and have been shown to have different neuronal roles. For instance, in hippocampus, mGlu$_1$ increases the frequency of spontaneous inhibitory postsynaptic currents, whereas mGlu$_5$ potentiates *N*-methyl-D-aspartate receptor currents (Mannaioni et al., 2001). In particular, mGlu$_5$ has been specifically implicated in a number of neuropsychiatric disorders including addiction, schizophrenia, fragile X syndrome, obsessive compulsive disorder, and Alzheimer's disease (Grueter et al., 2008; Michalon et al., 2012; Ronesi et al., 2012; Hu et al., 2014; Ade et al., 2016; Foster and Conn, 2017).

This work was supported by grants from the National Institutes of Health [R01-MH-063232] and [R01-NS-078291] to R.J.C., [F31-MH-109196] to C.R.M., [T32-DK-07563] to C.R.M.; and the American Heart Association [14PRE18420020] to X.W. and [15PRE25110020] to C.R.M. The content is solely the responsibility of the authors and does not necessarily represent the official views of the National Institutes of Health or other funding agencies. CRISPR/Cas9 pronuclear injections were performed by the Vanderbilt University School of Medicine Transgenic Mouse/ES Cell Shared Resource, which was supported through Cancer Center Support Grant CA68485, the Vanderbilt Diabetes Research and Training Center [DK020593], and the Center for Stem Cell Biology.
https://doi.org/10.1124/mol.118.113142.
[S] This article has supplemental material available at molpharm.aspetjournals.org.

ABBREVIATIONS: AM, acetoxymethyl ester; ANOVA, analysis of variance; bp, base pair; CA, constitutively active; CA-CaMKII, constitutively active Ca^{2+}/calmodulin-dependent protein kinase II; CaM, calmodulin; CaMKII, Ca^{2+}/calmodulin-dependent protein kinase II; CaMKAP, Ca^{2+}/calmodulin-dependent protein kinase II–associated protein; CTD, C-terminal domain; D_2R, D_2 dopamine receptor; D_3R, D_3 dopamine receptor; DMEM, Dulbecco's modified Eagle's medium; DTT, dithiothreitol; FBS, fetal bovine serum; F/F0, fluorescence intensity ratio; GST, glutathione *S*-transferase; HA, hemagglutinin; HEK293A, human embryonic kidney 293A; HRP, horseradish peroxidase; IR, infrared; KO, knockout; mApp, mApple control vector; mGlu, metabotropic glutamate receptor; PBS, phosphate-buffered saline; PKA, protein kinase A; PKC, protein kinase C; PMSF, phenylmethane sulfonyl fluoride; sulfo-NHS-SS-biotin, sulfosuccinimidyl 2-(biotinamido)-ethyl-1,3-dithiopropionate; TTBS, Tween Tris-buffered saline; WT, wild type.

Like $mGlu_5$, Ca^{2+}/calmodulin (CaM)-dependent protein kinase II α (CaMKIIα) is a key signaling protein in dendritic spines. CaMKIIα is activated by Ca^{2+}/CaM binding and undergoes autophosphorylation at Thr286 (Miller et al., 1988; Mukherji et al., 1994; Rich and Schulman, 1998; Yang and Schulman, 1999; Baucum et al., 2015). Thr286 autophosphorylation increases the affinity for Ca^{2+}/CaM and stabilizes the kinase in a constitutively active conformation. This constitutive activity is essential for normal synaptic plasticity in many brain regions (Silva et al., 1992a,b; Giese et al., 1998; Zhou et al., 2007; Mockett et al., 2011; Coultrap et al., 2014; Shonesy et al., 2014; Jin et al., 2015) including $mGlu_{1/5}$-dependent long-term depression in the hippocampus (Huber et al., 2001; Mockett et al., 2011). Interestingly, both CaMKIIα- and $mGlu_5$ knockout (KO) mice display deficits in learning and memory and hippocampal synaptic plasticity (Jia et al., 1998; Huber et al., 2001; Simonyi et al., 2005). Although both $mGlu_5$ and CaMKII are critical to many forms of plasticity, a functional link between the two has not been widely investigated.

The intracellular C-terminal domains (CTDs) of $mGlu_1$ and $mGlu_5$ have emerged as important loci for regulation by protein binding and phosphorylation (Enz, 2012; Mao and Wang, 2016). Although there are two splice variants of $mGlu_5$ ($mGlu_{5a}$ and $mGlu_{5b}$), most studies have focused on $mGlu_{5a}$, and a few pharmacological differences between splice variants have been identified (Joly et al., 1995; Minakami et al., 1995; Romano et al., 1996). The $mGlu_5$-CTD has been shown to bind to a number of different proteins including Ca^{2+}/CaM and Homer to regulate cell-surface expression of the receptor (Roche et al., 1999; Saito et al., 2002; Lee et al., 2008; Choi et al., 2011). Protein kinase A (PKA) and protein kinase C (PKC) also regulate $mGlu_5$ surface expression through phosphorylation of the CTD (Mao et al., 2008; Uematsu et al., 2015). It was recently reported that CaMKII can bind to the CTD and intracellular loop 2 of both $mGlu_1$ and $mGlu_5$ (Jin et al., 2013a,b; Raka et al., 2015) and that CaMKII modulates $mGlu_5$ agonist-induced internalization and ERK1/2 activation (Raka et al., 2015). Here, we identify three basic residues (Lys^{866}-Arg^{877}-Arg^{888}) in the membrane proximal region of the $mGlu_{5a}$-CTD that are essential for a direct interaction with activated CaMKIIα, and provide novel insights into multiple factors that modulate the interaction. We also show that CaMKII binding to the CTD is important for the regulation of $mGlu_5$ surface expression and Ca^{2+} mobilization. These data provide novel insights into the molecular basis and function of the $mGlu_5$-CaMKII interaction that may be involved in synaptic plasticity.

Materials and Methods

DNA Constructs

The glutathione *S*-transferase (GST)-$mGlu_{5a}$-CTD expression construct was created by polymerase chain reaction amplification of the region encoding residues 827–964 of $mGlu_{5a}$ (NP_058708.1) using forward primer 5′-CTGGAAGTTCTGTTCCAGGGGCCCGGATCCAAACCGGAGAGAAAT-3′ and reverse primer 5′-GCCGCAAGCTTGTCGACGGAGCTCGAATTCTTAGGTCCCAAAGCGCTT-3′ and inserting the product into BamHI/EcoR1 sites of pGEX6P using a sequence- and ligation-independent cloning protocol (Li and Elledge, 2012).

The pCGN plasmid to express wild-type (WT) $mGlu_{5a}$ with an N-terminal hemagglutinin (HA) tag was made by amplifying the entire rat $mGlu_{5a}$ coding sequence (forward primer: 5′-TGACGTGCCTGACTATGCCTCTAGAATGGTCCTTCTGTTGATCCT-3′; reverse primer: 5′-ACTCACCCTGAAGTTCTCAGGATCCTCACAACGATGAAGAACTCT-3′) and inserting the fragment into XbaI and BamHI restriction sites of the empty pCGN plasmid [a gift from Dr. Winship Herr, Université de Lausanne, Switzerland; Addgene (Cambridge, MA) plasmid ID 53308].

The $K^{866}RR^{868}$ mutation to AAA in $mGlu_{5a}$ was generated by site-directed mutagenesis of the pGEX6P or pCGN constructs (see above) using a Quick Change protocol (Agilent Technologies, Santa Clara, CA) with the following primers: forward, 5′-GGGTTTCCCCAGAGGAG-C**CGGCGGCGG**CCCACAGGTTGACTAGGCTGCT-3′; and reverse, 5′-AGCAGCCTAGTCAACCTGTGGG**CCGCCGCCGG**CTCCTCTG-GGGAAACCC-3′.

We used pcDNA3.1 constructs to express untagged and mApple-tagged WT-CaMKIIα and a constitutively active (CA) T286D/T305A/T306A triple mutant of CaMKIIα (CA-CaMKIIα), as previously described (Jiao et al., 2008; Jalan-Sakrikar et al., 2012; Stephenson et al., 2017). In the CA-CaMKIIα, the phospho-mimetic T286D mutation results in constitutive CaMKIIα activity and the phospho-null T305A/T306A mutations prevent CaMKIIα phosphorylation at these sites, which interferes with binding of Ca^{2+}/CaM and α-actinin (Jalan-Sakrikar et al., 2012).

Recombinant Protein Purification

Expression and purification of recombinant mouse CaMKIIα has been described before (McNeill and Colbran, 1995). To express GST-tagged proteins, pGEX6P-1 plasmids were transformed into BL21(DE3) bacteria cells. Cells were grown in Lysogeny broth media at 37°C to reach an optical density of ~0.6. Cells were cooled to room temperature, and isopropyl β-D-1-thiogalactopyranoside (0.2 mM) was then added to induce protein expression for 12–16 hours. Inducing protein expression at room temperature substantially reduced the protein degradation seen when proteins were expressed at 37°C. Expressed proteins were purified using Pierce Glutathione Agarose Beads (cat. no. 16101; Thermo Fisher Scientific, Waltham, MA) following manufacturer instructions. Eluted proteins were then dialyzed in 10 mM HEPES pH 7.5, 25 μM phenylmethane sulfonyl fluoride (PMSF), 62.5 μM benzamidine, 62.5 μM EDTA, and 0.1% Triton X-100 overnight with one buffer change.

CaMKIIα Autophosphorylation

Purified mouse CaMKIIα was autophosphorylated under two different conditions. Typically, CaMKIIα was incubated with 50 mM HEPES, pH 7.5, 10 mM $Mg(CH_3\text{-}COO)_2$, 0.5 mM $CaCl_2$, 2 μM CaM, and 40 μM ATP on ice for 90 seconds before the addition of EDTA and EGTA (20 mM final) to terminate phosphorylation by chelation of Mg^{2+} and Ca^{2+}. Similar conditions were previously shown to result in the selective autophosphorylation of Thr286 (McNeill and Colbran, 1995). Where indicated, identical autophosphorylation reactions were incubated for 10 minutes at 30°C to perform a more extensive phosphorylation at several additional sites (Baucum et al., 2015).

GST Pull-Down and CaM Binding Competition

Purified GST-$mGlu_5$-CTD (1 μM) and CaMKIIα (62.5 nM; preautophosphorylated as indicated in the figure legends) were incubated at 4°C in GST pull-down buffer [50 mM Tris-HCl pH 7.5; 150 mM NaCl; 1% (v/v) Triton X-100] with either 2 mM EGTA or 2.5 mM $CaCl_2$ plus 10 μM CaM, as indicated. An aliquot (5%) of each incubation was saved as an input sample. After 1 hour, prewashed Pierce Glutathione Agarose Beads (cat. no. 16101; Thermo Fisher Scientific) (15 μl of a 50: 50 slurry) were added, and incubation was continued at 4°C for an additional 1 hour. The beads were then separated by centrifugation (2000*g*, 30 seconds) and washed three times with GST pull-down buffer containing either 2 mM EGTA or 2.5 mM $CaCl_2$, respectively. Beads were then incubated at 4°C with GST pull-down buffer containing 20 mM glutathione, adjusted to pH 8.0, for 10 minutes. After centrifugation, eluted proteins were transferred to a new tube, mixed with 4× SDS-PAGE buffer and heated for 10 minutes at 90°C prior to SDS-PAGE and Western blot analysis.

Cell Culture, Transfection and Immunoprecipitation

HEK293A cells (cat. no. R70507; Thermo Fisher Scientific) were maintained in complete Dulbecco's modified Eagle's medium (DMEM) supplemented with 5% fetal bovine serum (FBS), 2 mM L-glutamine, 20 mM HEPES, 0.1 mM nonessential amino acids, and 1 mM sodium pyruvate, at 37°C in a humidified incubator containing 5% CO_2 and 95% O_2. Vectors encoding mApple-CaMKIIα (WT or CA) and $mGlu_{5a}$ (3 μg DNA each) or empty vector controls (3 μg) were cotransfected into one 10-cm dish of 60%–70% confluent HEK293A cells using 3 μl/μg DNA of Fugene 6 (cat. no. E2691; Promega, Madison, WI). About 48 hours later, cells were lysed in 50 mM Tris-HCl pH 7.5, 150 mM NaCl, 1 mM EDTA, 1 mM EGTA, 1 mM dithiothreitol (DTT), 0.5% NP40 (v/v), 0.5% deoxycholate (v/v), 0.2 mm PMSF, 1 mm benzamidine, 10 μg/ml leupeptin, 10 μm pepstatin, and 1 μm microcystin. Cell lysates were cleared by centrifugation (10 minutes at 12,000*g*), and a 30 μl sample of the input was saved for SDS-PAGE. The remaining supernatant was incubated at 4°C for 1 hour with rabbit anti-HA antibodies and 20 μl prewashed Dynabeads Protein A (50% v/v; cat. no. 10001D; Thermo Fisher Scientific). Beads were isolated magnetically, washed three times using lysis buffer, and eluted using 2× Laemmli sample buffer for 10 minutes at room temperature prior to SDS-PAGE and Western blotting.

Biotinylation and Cell Surface Expression

Transfected HEK293A cells (see above) were placed on ice, the media were gently removed, and the cells were immediately washed two times using ice-cold phosphate-buffered saline (PBS). Cells were then scraped into ice-cold PBS, transferred to a 1.5-ml tube, centrifuged at 4°C (500*g*; 3 minutes), and gently resuspended in 1 ml of cold PBS containing 2 mg of EZ-Link sulfo-NHS-SS-biotin (ThermoFisher). After gently rocking for 1 hour, excess reagent was quenched by the addition of 50 mM Tris HCl, pH 8.0, and cells were centrifuged and washed again in 1 ml of 50 mM Tris HCl. Cells were then suspended in 1 ml of ice-cold lysis buffer (25 mM Tris HCl, pH 7.4; 150 mM NaCl; 1% NP40; 0.5% sodium deoxycholate containing 0.2 mm PMSF; 1 mm benzamidine; 10 μg/ml leupeptin; and 10 μm pepstatin) and incubated on ice for 30 minutes. Insoluble material was removed by centrifugation (16,000*g*; 10 minutes, at 4°C), and a 30-μl aliquot of the supernatant was saved for an input sample for SDS-PAGE (Cho et al., 2014). The remaining supernatants were mixed for 1 hour at 4°C with magnetic NeutrAvidin beads (30 μl; 50% slurry; Thermo Fisher Scientific). The beads were separated magnetically and washed three times with lysis buffer. Biotinylated proteins were dissociated from the beads in SDS sample buffer containing 150 mM DTT for 10 minutes at room temperature. The biotinylated and total protein samples were analyzed by Western blotting for $mGlu_5$.

Immunoblotting and Semiquantitative Analysis

Since heating samples results in aggregation of full-length $mGlu_5$ protein, all samples that were blotted for the full-length receptor were incubated for 10 minutes at room temperature before SDS-PAGE. SDS-polyacrylamide gels were transferred to nylon-backed nitrocellulose membranes in 10 mM 3-(cyclohexylamino)propanesulfonic acid buffer. After blocking in Tween Tris-buffered saline [TTBS; 50 mm Tris-HCl, pH 7.5, 0.1% (v/v) Tween 20, 150 mm NaCl] containing 5% nonfat milk, membranes were incubated for either 2 hours at room temperature for purified protein studies or overnight at 4°C in HEK293A cell and brain lysate samples with primary antibodies diluted in TTBS with 5% milk. Membranes were washed five times in TTBS and incubated for 1 hour at room temperature with secondary antibodies conjugated to horseradish peroxidase (HRP) (Promega; or Santa Cruz Biotechnology, Dallas, TX), or infrared (IR) dyes (LI-COR Biosciences, Lincoln, NE) diluted in TTBS with 5% milk. Antibody signals were visualized via enzyme-linked chemiluminescence using the Western Lightning Plus-ECL enhanced chemiluminescent substrate (PerkinElmer, Waltham, MA) and visualized using Premium X-ray Film (Phenix Research Products, Candler, NC). Secondary antibodies conjugated to IR dyes (LI-COR Biosciences) were used for development with an Odyssey System (LI-COR Biosciences). Images were quantified using ImageJ software.

Antibodies

The following antibodies were used for immunoblotting at the indicated dilutions: total CaMKIIα (1:5000; cat. no. MA1-048; Thermo Fisher Scientific) and p-Thr286 CaMKIIα (1:3000; cat. no. sc-12886-R; Santa Cruz Biotechnology); $mGlu_5$-specific antibody (1:3000; cat. no. AB5675; MilliporeSigma, Burlington, MA); rabbit anti-HA (5 μl for immunoprecipitation; cat. no. sc805; Santa Cruz Biotechnology); and goat-GST antibody (1:10,000; cat. no. ab181652; Abcam, Cambridge, UK).

Secondary Antibodies. Secondary antibodies were as follows: HRP-conjugated anti-rabbit (1:3000; cat. no. W4011; Promega), HRP-conjugated anti-mouse (1:3000; cat. no. W4021; Promega), and HRP-conjugated anti-goat (1:3000; cat. no. sc-2056; Santa Cruz Biotechnology); IR dye–conjugated donkey anti-rabbit 800CW (1:10,000; cat. no. 926–32213; LI-COR Biosciences), and IR dye–conjugated donkey anti-mouse 680LT (1:10,000; cat. no. 926–68022; LI-COR Biosciences).

Mice

CaMKII-KO mice were generated in the Vanderbilt Transgenic Mouse Core as a by-product of published CRISPR/Cas9-mediated experiments directed at creating a knockin E183V mutation of CaMKIIα (Stephenson et al., 2017). We selected a founder containing a deletion of 11 base pairs (bp) (TGCTGAGGAAG) from exon 8, leading to a frame shift and early translational termination. Primers used to genotype the CaMKIIα KO mice are as follows: forward, 5′-GATACCTCTCCCCAGAAGGAC-3′, reverse, 5′-TGCAGTGGTAAGGAGTGGTG-3′ for WT; and forward, 5′-GGACAGTACAACCCCAGCTT-3′, and reverse, 5′-CCCGTACGGGTCCTTCCTCA-3′ for KO, generating a 206-bp band for WT, a 351-bp band for KO, and a 557-bp band for all mice. The CaMKIIα KO was confirmed by immunoblotting brain lysates. All mice were on a mixed B6D2 [C57BL/6J (B6) × DBA/2J (D2)] background and were housed (2–5 per cage) on a 12-hour light/dark cycle with food and water ad libitum. WT and KO experimental mice (littermates) were generated using an HETXHET breeding strategy. All animal procedures were approved by the Vanderbilt University Institutional Animal Care and Use Committee in accordance with the National Institutes of Health *Guide for the Care and Use of Laboratory Animals*.

Mouse Brain Tissue Preparation and Immunoprecipitation

Both male and female mice (30-60 days old) were anesthetized with isoflurane and decapitated, and forebrains were quickly dissected. Half of a forebrain (cut along the mid-line) was homogenized using at least 20 strokes with a dounce homogenizer in 1.5 ml of an isotonic buffer containing 150 mM KCl, 50 mM Tris-HCl, 1 mm DTT, 1% (v/v) Triton X-100, 1% sodium deoxycholate, 0.2 mM PMSF, 1 mM benzamidine, 10 μg/ml leupeptin, 10 μM pepstatin, and 1 μM microcystin. The homogenate was rotated end over end at 4°C for 30 minutes and then centrifuged at 10,000*g* for 30 minutes to remove insoluble material. A 30-μl input sample was saved before CaMKIIα (MA1-048) antibody, and 20 μl of magnetic Protein G beads (cat. no. 10003D; Invitrogen) were added to 1 ml of homogenate and rotated end over end for 3–4 hours. Beads were separated magnetically and washed three times with homogenization buffer. Immunoprecipitated complexes were eluted using 2× Lamelli Sample Buffer containing 150 mM DTT for 10 minutes at room temperature and analyzed by immunoblotting.

Ca^{2+} Imaging in 96-Well Plates

A FlexStation II liquid handler/plate reader (Molecular Devices, Sunnyvale, CA) was used for intracellular Ca^{2+} measurements in HEK293A cells stably expressing low amounts of the rat $mGlu_{5a}$

receptor (*293A-5a^{LOW}* cells), as previously described (Hammond et al., 2010; Gregory et al., 2012; Noetzel et al., 2012). The cells were maintained at 37°C in complete DMEM supplemented with 10% FBS, 2 mM L-glutamine, 20 mM HEPES pH 7.5, 0.1 mM nonessential amino acids, 1 mM sodium pyruvate, antibiotic/antimycotic solution (Thermo Fisher Scientific), and 500 μg/ml G418 in a humidified incubator containing 5% CO_2/95% O_2. For experiments, 10-cm dishes were transfected with 3 μg of mApple control vector (mApp) or 3 μg of mApp-CaMKIIα (WT or CA; see above). On the following day, cells were transferred to clear-bottomed, black-walled, poly-D-lysine–coated 96-well plates (BD BioCoat; BD Biosciences, San Jose, CA) (3×10^4 cells/well) in DMEM containing 10% dialyzed FBS, 20 mM HEPES, 1 mM sodium pyruvate, and incubated overnight at 37°C in 5% CO_2. Approximately 24 hours later, medium was manually removed and replaced with Hanks' balanced salt solution containing 20 mM HEPES, 2.5 mM probenecid, and 2 μM Fluo-4/acetoxymethyl ester (AM) dye (pH 7.4), and plates were incubated for 30 minutes (37°C, 5% CO_2). This medium was manually removed and replaced with 40 μl of calcium assay buffer (Hanks' balanced salt solution, 20 mM HEPES, and 2.5 mM probenecid, pH 7.4). Glutamate additions were performed after a 30-second baseline to construct concentration-response curves, and plates were monitored for a total of 120 seconds using an excitation wavelength of 488 nm, an emission wavelength of 525 nm, and a cutoff wavelength of 515 nm. Data were collected with SoftMax Pro (Molecular Devices) then transformed, and agonist concentration-response curves were fitted to a four-parameter logistic equation with GraphPad Prism (GraphPad Software, San Diego, CA). For area under the curve measurements, time parameters were set to measure the area under the curve between the time points of 10–60 seconds to capture the initial Ca^{2+} peak. Raw values were generated by SoftMax Pro and normalized to the maximum response of control cells.

Single Cell Ca^{2+} Imaging

HEK293A cells were transiently transfected to express full-length $mGlu_{5a}$ (WT or mutated as indicated: 0.3 μg DNA) and either mApple or mApple-CA-CaMKIIα (3 μg DNA). On the following day, transfected cells were plated in clear glass-bottomed, poly-D-lysine–coated 29 mM dishes (D29-10-1.5-N; Cellvis, Mountain View, CA) (5×10^4 cells) in DMEM containing 10% dialyzed FBS, 20 mM HEPES, 1 mM sodium pyruvate, and 1% penicillin/streptomycin (Thermo Fisher Scientific) and incubated overnight at 37°C in 5% CO_2. On the day of the experiment, cells were incubated in media supplemented with 2 μM Fura-2/AM (Thermo Fisher Scientific) for 20 minutes at 37°C in 5% CO_2, and then transferred to a Ca^{2+} imaging solution (150 mM NaCl, 5 mM KCl, 2 mM $CaCl_2$, 2 mM $MgCl_2$, 10 mM glucose, and 10 mM HEPES; at pH 7.5 and ~313 mOsm). After incubation for 20 minutes at 37°C in 5% CO_2, fluorescence imaging was performed using a Nikon (Tokyo, Japan) Eclipse TE2000-U Microscope equipped with an epifluorescence illuminator (Sutter Instrument, Novato, CA), a charge-coupled device camera (model HQ2; Photometrics, Tucson, AZ), and Nikon Elements software. Cells were perfused at 37°C at a flow rate of 2 ml/min with Ca^{2+} imaging solution. First, the field of view was imaged using 568-nm excitation to detect cells expressing mApple. Then, ratios of emitted fluorescence (at 510 nm) from mApple-positive cells were measured after excitation at 340 and 380 nm (F340/F380); ratios were measured every 3 seconds for a 1-minute baseline period. Then the cells were treated with 100 μM glutamate (added to the Ca^{2+} imaging solution) for 10 minutes, during which time the Fura-2 F340/F380 ratios were collected every 3 seconds. Relative changes in Ca^{2+} levels of the mApple-expressing cells were analyzed using Nikon Elements software. The F340/F380 ratios of each cell were normalized to the first F340/F380 ratio acquired for that cell during the baseline period [fluorescence intensity ratio (F/F0) = (340/380 value)/(baseline 340/380 value)] and then analyzed using Clampfit software (Molecular Devices). Peak Ca^{2+} responses for all cells were aligned (at 45 seconds), a ROUT test was first used to identify outliers in the maximal ΔF/F0 values for all cells within each experimental group, and then ΔF/F0 values for each time point were averaged together for each dish of cells. The maximal Ca^{2+} response was defined as the average of all the peak ΔF/F0 values on an experimental day. An average trace for each day of experiments was generated to calculate the half-life of the Ca^{2+} signal; the decline of the average ΔF/F0 values in each dish were normalized to the average maximal Ca^{2+} response in that dish and then fitted to a nonlinear one-phase exponential decay fit constrained to $y0 = 1$ using GraphPad Prism version 6.0. We determined ΔF/F0 and half-lives in five independent experiments (transfections) on separate days (19–124 cells/condition per day) and tested for differences using a Student's *t* test. All values are presented as the mean ± S.E.M.

Results

Mouse Forebrain Lysates Contain CaMKIIα-$mGlu_5$ Complexes. To confirm that $mGlu_5$ specifically associates with CaMKII in the brain, we incubated forebrain lysates from WT or CaMKIIα-KO mice with a CaMKIIα-specific monoclonal antibody or a control IgG. The resulting immune complexes were isolated and then immunoblotted for $mGlu_5$ and CaMKIIα. Note that the $mGlu_5$ antibody used for these studies recognizes an epitope that is shared by the two known $mGlu_5$ splice variants, $mGlu_{5a}$ and $mGlu_{5b}$, which are differentially expressed during development (Minakami et al., 1995; Romano et al., 1996). Input samples from WT and CaMKIIα KO tissue prepared in parallel contain similar levels of the monomeric and dimeric forms of $mGlu_5$ (Fig. 1), although the ratio of monomeric and dimeric species varied between independent experiments (data not shown). CaMKIIα complexes isolated from WT mouse forebrain contained both monomeric and dimeric forms of $mGlu_5$, with the ratio of these forms reflecting variability in the ratio detected in the inputs. However, very little $mGlu_5$ could be detected in IgG control complexes isolated from WT tissue, or in CaMKIIα complexes isolated from CaMKIIα KO tissue (Fig. 1). Thus, $mGlu_5$ is a bona fide component of the CaMKIIα complexes present in mouse brain lysates.

CaMKIIα Directly Binds to the $mGlu_5$ C-Terminal Domain. Like most prior studies, we chose to use the $mGlu_{5a}$ splice variant for our molecular studies. It was previously

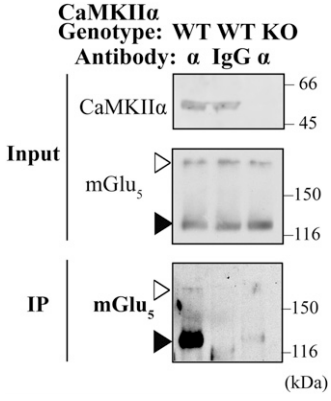

Fig. 1. Coimmunoprecipitation of $mGlu_5$ with mouse forebrain CaMKIIα. Solubilized fractions from WT or CaMKIIα KO mouse forebrain were immunoprecipitated (IP) using CaMKIIα-specific (α) or control (IgG) antibodies, as indicated. Inputs and immune complexes were analyzed by immunoblotting: mGlu5 was detected only in immune complexes isolated from WT tissue using the CaMKIIα antibody. Open and closed arrowheads indicate dimeric and monomeric species of $mGlu_5$. The figure is representative of three similar experiments.

reported that residues 827–964 of the $mGlu_{5a}$-CTD bind to inactive CaMKIIα, but that CaMKII autophosphorylation disrupted the interaction (Jin et al., 2013b). To confirm this finding, we generated a GST-tagged $mGlu_{5a}$-CTD construct containing residues 827–964 (GST-$mGlu_{5a}$-CTD) for use in glutathione agarose cosedimentation experiments. Initial studies detected weak binding of inactive CaMKIIα to GST-$mGlu_{5a}$-CTD that was not consistently above background binding to a GST negative control (data not shown). Therefore, we systematically tested interactions of GST-$mGlu_{5a}$-CTD with CaMKIIα in various activation states.

Purified CaMKIIα was autophosphorylated in the presence of Ca^{2+}/CaM in vitro at either 4°C or 30°C. Similar total levels of Thr286 autophosphorylation were detected by immunoblotting after incubation at either 4°C or 30°C (Fig. 2A), but the 30°C autophosphorylation reduced the electrophoretic mobility of CaMKIIα. These observations are consistent with those of prior studies showing that incubation at 4°C results in selective Thr286 autophosphorylation (McNeill and Colbran, 1995), whereas incubation at 30°C allows for extensive autophosphorylation at several other sites (Baucum et al., 2015).

We then performed glutathione-agarose cosedimentation experiments to test the interaction of GST-$mGlu_5$-CTD with CaMKIIα in these different activation states (after terminating the autophosphorylation reactions by chelating metal ions with excess EGTA and EDTA). The selective Thr286-autophosphorylation (4°C) protocol resulted in a robust enhancement of CaMKIIα binding to GST-$mGlu_5$-CTD relative to the nonphosphorylated kinase, but this interaction was substantially reduced after more extensive in vitro phosphorylation at 30°C (Fig. 2B). The short exposure times used for the development of these immunoblots failed to detect weak binding of inactive CaMKIIα to GST-$mGlu_5$-CTD. In combination, these data show that although activation and Thr286 autophosphorylation of CaMKIIα strongly enhance binding to the $mGlu_{5a}$-CTD, the interaction can be reduced by autophosphorylation at additional non-Thr286 sites.

Binding of Activated CaMKIIα to the GST-$mGlu_{5a}$-CTD Is Disrupted by Ca^{2+}/CaM. Ca^{2+}/CaM binds to residues 889–917 within the CTD of $mGlu_{5a}$ with important functional consequences (Minakami et al., 1997; Lee et al., 2008; Choi et al., 2011). Moreover, it was previously reported that excess Ca^{2+}/CaM disrupts the binding of inactive

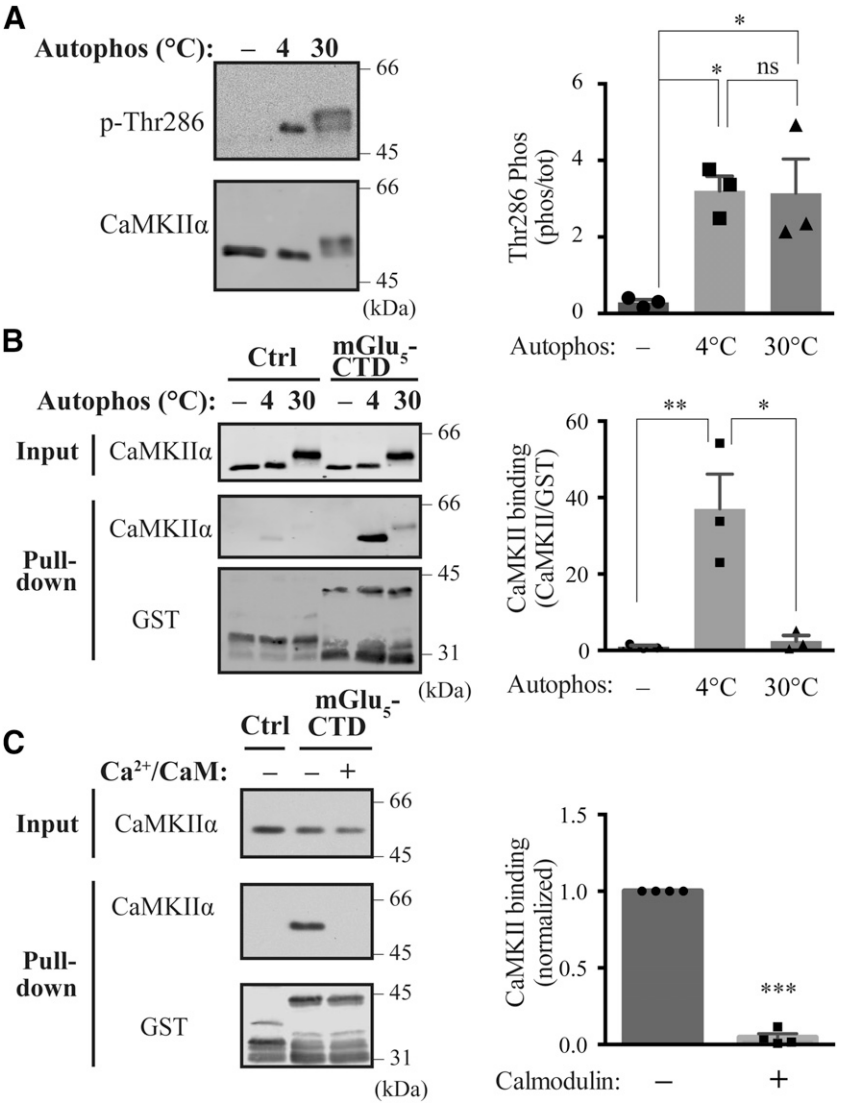

Fig. 2. CaMKII autophosphorylation at Thr286 enhances binding to the $mGlu_5$ CTD. (A) Autophosphorylation (Autophos) of purified CaMKIIα. Purified CaMKIIα was incubated with $Mg(C_2H_3O_2)_2$, $CaCl_2$, CaM, and ATP for either 90 seconds at 4°C or 10 minutes at 30°C, and samples were immunoblotted for total or phospho-Thr286 (p-Thr286) CaMKII. Although quantitative analysis (right) indicated that there was a similarly robust Thr286 autophosphorylation using these two conditions, the 10-minute/30°C incubation resulted in a substantial reduction in electrophoretic mobility due to phosphorylation at additional unidentified sites. Data are plotted as the mean ± S.E.M. ($n = 3$) and analyzed using a one-way ANOVA ($P = 0.0167$, $F = 8.746$, $R^2 = 0.7446$) with Sidak's post hoc test for multiplicity adjusted P values: control (Ctrl) vs. 4°C, $P = 0.031$; control vs. 30°C, $P = 0.035$; 4°C vs. 30°C, $P = 1.00$. (B) The GST-$mGlu_{5a}$-CTD binds CaMKIIα after selective autophosphorylation at Thr286. GST-$mGlu_{5a}$-CTD was incubated with purified CaMKIIα that had been preincubated as in (A), and complexes were isolated using glutathione agarose. Immunoblot analyses revealed that CaMKIIα binding to the CTD was strongly enhanced by selective Thr286 autophosphorylation at 4°C, but that the autophosphorylation of additional sites on CaMKII at 30°C substantially reduced binding. Data are plotted as the mean ± S.E.M. ($n = 3$) and were analyzed using a one-way ANOVA ($P = 0.005$, $F = 2.477$, $R^2 = 0.829$) with Sidak's post hoc test for multiplicity-adjusted P values: control vs. 4°C, $P = 0.009$; 4°C vs. 30°C, $P = 0.011$; control vs. 30°C, $P = 1.00$. (C) Binding of activated CaMKIIα to GST-$mGlu_{5a}$-CTD is disrupted by Ca^{2+}/CaM. Purified CaMKIIα was autophosphorylated for 90 seconds at 4°C [see (A)] and then incubated with GST-$mGlu_{5a}$-CTD in the absence or presence of excess Ca^{2+}/CaM (see *Materials and Methods*). Complexes were isolated using glutathione-agarose and then immunoblotted as indicated. Data are plotted as the mean ± S.E.M.; excess Ca^{2+}/CaM significantly reduced CaMKIIα binding ($P < 0.0001$ relative to a theoretical value of 1.00, one-sample t test; $n = 4$). In all panels, the symbols *, ** and *** indicate $P < 0.05$, 0.01 and 0.001, respectively, with n.s. indicating non-significant ($P > 0.05$).

CaMKIIα to the $mGlu_{5a}$-CTD (Jin et al., 2013b). Therefore, we tested whether excess Ca^{2+}/CaM also disrupts the binding of activated CaMKIIα to GST-$mGlu_{5a}$-CTD. Thr286-autophosphorylated CaMKIIα (4°C protocol) robustly binds to GST-$mGlu_{5a}$-CTD, as noted above, but this interaction was essentially eliminated by the inclusion of excess Ca^{2+}/CaM in the binding assay (Fig. 2C). Thus, binding of activated CaMKIIα to the $mGlu_{5a}$ CTD is also blocked by Ca^{2+}/CaM, suggesting that multiple Ca^{2+}-sensitive proteins are involved in the regulation of $mGlu_5$ signaling.

Identification of a CaMKIIα-Binding Determinant in the $mGlu_5$ CTD. As an initial approach to identify key CaMKIIα-binding determinants in the $mGlu_{5a}$ CTD, we compared residues 827–964 of $mGlu_5$ with CaMKIIα-binding domains that have been previously identified in other proteins. Our laboratory recently showed that activated CaMKIIα binds to the N-terminal domains of $Ca_V1.2$ and $Ca_V1.3$ L-type voltage-gated Ca^{2+} channels, and that this interaction is disrupted by the mutation of three basic residues (Arg^{83}-Lys-Arg^{85}) to alanine (Wang et al., 2017). Similar tribasic residue motifs are also present within CaMKIIα-binding domains that have been previously identified in the intracellular loops of the D_2 dopamine receptor (D_2R) and D_3 dopamine receptor (D_3R) (Liu et al., 2009; Zhang et al., 2014) and the $mGlu_1$-CTD (Jin et al., 2013a). Notably, the CaMKIIα-binding fragment of the $mGlu_{5a}$-CTD also contains a tribasic residue motif (residues Lys^{866}-Arg^{867}-Arg^{868}) (Fig. 3A). We found that substituting alanines for Lys^{866}-Arg^{867}-Arg^{868} in the $mGlu_{5a}$-CTD essentially abolished the binding of activated CaMKIIα to GST-$mGlu_5$-CTD in vitro (Fig. 3B). These data identify a key determinant for CaMKII binding to the CTD of $mGlu_{5a}$.

CaMKIIα Activation Increases CaMKIIα-$mGlu_{5a}$ Association in Heterologous Cells. To better understand the interaction of CaMKIIα with full-length $mGlu_{5a}$ we conducted coimmunoprecipitation experiments from lysates of transfected HEK293A cells. We first tested the hypothesis that CaMKIIα activation would increase the association with full-length $mGlu_{5a}$, as with in vitro binding of CaMKIIα to GST-$mGlu_{5a}$-CTD. We expressed mApple-tagged WT CaMKIIα in the absence or presence of $mGlu_{5a}$ with an N-terminal HA-epitope tag in HEK293A cells. Prior to HA immunoprecipitation, the cell lysates were split into two aliquots and preincubated with either excess EGTA and EDTA or with Ca^{2+}/CaM, Mg^{2+}, ATP, and phosphatase inhibitors to stimulate CaMKIIα autophosphorylation. CaMKII activation in the lysates resulted in a robust increase in autophosphorylation at Thr286, without the large shift in electrophoretic mobility that was observed after autophosphorylation of purified CaMKIIα at 30°C (Fig. 4A). HA-immunoprecipitation from the two preincubated lysates yielded similar amounts of the monomeric and dimeric species of HA-$mGlu_{5a}$, but CaMKIIα activation resulted in a statistically significant ~3-fold increase in the amount of coimmunoprecipitated CaMKIIα (Fig. 4A). These data show that full-length $mGlu_{5a}$ preferentially interacts with activated WT CaMKIIα.

Association of Activated CaMKIIα with Full-Length $mGlu_{5a}$ Requires Arg^{83}-Lys-Arg^{85}. We next investigated whether the association of activated CaMKIIα with full-length $mGlu_{5a}$ involves the CTD. To avoid complications that might arise from preincubating cell lysates to activate WT-CaMKIIα, we used an mApple-tagged CA-CaMKIIα (mApple-CA-CaMKIIα); the phosphomimetic T286D mutation results in constitutive CaMKIIα activity, and the phospho-null T305A/T306A mutations prevent CaMKIIα phosphorylation at these sites, which interferes with the binding of Ca^{2+}/CaM and α-actinin (Jalan-Sakrikar et al., 2012). The mApple-CA-CaMKIIα was expressed alone, or coexpressed with either HA-$mGlu_{5a}$ or HA-$mGlu_{5a}$-AAA (with Lys^{866}-Arg^{867}-Arg^{868} mutated to alanines). HA-immunoprecipitation from cell lysates confirmed a robust association of mApple-CA-CaMKIIα with WT $mGlu_{5a}$ that was partially (~50%) reduced by the triple alanine mutation in the CTD (Fig. 4B). These data demonstrate that the Lys^{866}-Arg^{867}-Arg^{868} residues in the $mGlu_{5a}$-CTD play an important role in the association of activated CaMKIIα with the full-length $mGlu_5$ receptor.

CaMKIIα Increases Basal $mGlu_{5a}$ Surface Expression. Since the CTD is known to modulate $mGlu_5$ cell-surface expression and consequently $mGlu_5$ signaling, we investigated the effect of CaMKIIα on the cell-surface expression of full-length $mGlu_{5a}$. Intact HEK293A cells expressing $mGlu_5$ with or without mApple-CA-CaMKIIα were incubated with sulfo-NHS-SS-biotin to biotinylate all surface-expressed proteins. Streptavidin-conjugated magnetic beads were then used to isolate cell-surface proteins from cell lysates. Immunoblotting of total cell lysates and isolated cell-surface proteins revealed that the coexpression of mApple-CA-CaMKIIα increased the proportion of $mGlu_{5a}$ expressed on the cell surface by 3.0 ± 0.7-fold (S.E.M.) under basal conditions (P = 0.036; one-

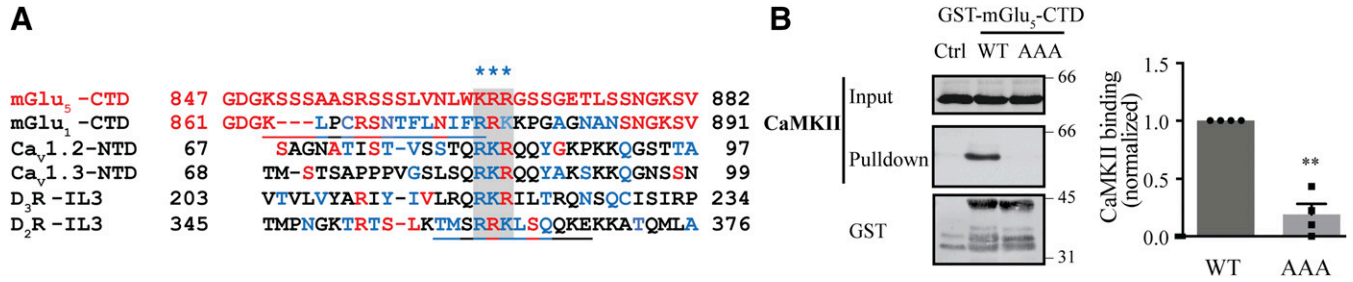

Fig. 3. Identification of CaMKII-binding determinants in the $mGlu_{5a}$-CTD. (A) Alignment of part of the $mGlu_{5a}$-CTD with amino acid sequences surrounding known CaMKII-binding domains. Tribasic residue motifs (highlighted with blue asterisks above) were identified within CaMKII-binding domains from other proteins, as well as within the CaMKII binding fragment in the CTD of $mGlu_{5a}$. Mutation of $R^{83}K^{84}R^{85}$ to AAA in the $Ca_V1.3$ N-terminal domain disrupts the binding of CaMKII (Wang et al., 2017). The red and blue fonts indicate residues in each domain that are identical and homologous, respectively, with residues in the $mGlu_{5a}$ sequence. Underlined residues in the $mGlu_1$-CTD and the D_2R and D_3R (IL3, third intracellular loop) demark the sequences of synthetic peptides that were shown to compete for CaMKII binding (Jin et al., 2013a; Zhang et al., 2014). (B) Mutation of the tribasic residue motif in the $mGlu_{5a}$-CTD disrupts CaMKII binding. Thr286 autophosphorylated CaMKIIα (90 seconds/4°C protocol) was incubated with GST-$mGlu_{5a}$-CTD (WT or with a $K^{866}R^{867}R^{868}$ to AAA mutation), and complexes were analyzed as in Fig. 1. The $K^{866}R^{867}R^{868}$/AAA mutation essentially abolishes CaMKII binding. Data are plotted as the mean ± S.E.M. (P = 0.003, one-sample t test; n = 4). In panel B, the symbol ** indicates $P<0.01$.

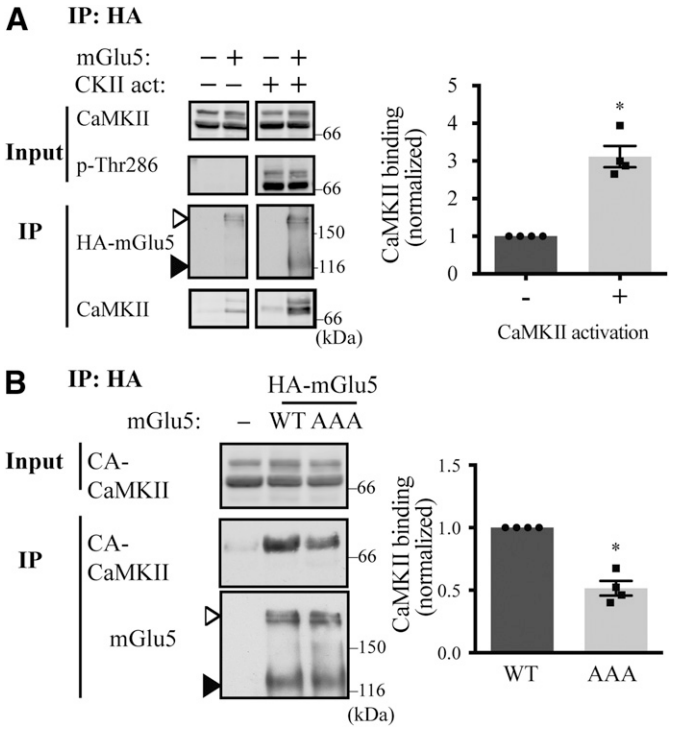

Fig. 4. Role of the CTD in full-length $mGlu_{5a}$ binding to activated CaMKIIα. (A) CaMKII activation enhances interaction with full length $mGlu_5$. Solubilized fractions of HEK293A cells expressing HA-tagged $mGlu_{5a}$ and/or mApple-tagged WT CaMKIIα (as indicated above lanes) were pre-incubated with Ca^{2+}/CaM, $MgAc_2$, and ATP in the presence or absence of excess EDTA (± activation, respectively) and then immunoprecipitated (IP) using antibodies to the HA epitope. Lysates and immune complexes were analyzed by immunoblotting, as indicated. CaMKIIα activation results in robust Thr-286 autophosphorylation, which increases CaMKIIα association with HA-$mGlu_{5a}$. Data are plotted as the mean ± S.E.M. ($P = 0.043$, one-sample t test; $n = 4$). Open and closed arrowheads indicate dimeric and monomeric species of $mGlu_{5a}$. (B) CaMKII association with full-length $mGlu_{5a}$ is disrupted by mutation of the CTD tribasic residue motif. Solubilized fractions of HEK293A cells expressing HA-$mGlu_5$ (WT or with the $K^{866}R^{867}R^{868}$/AAA mutation) and mApple-tagged CA-CaMKIIα were immunoprecipitated using antibodies to the HA epitope. Lysates and the immune complexes were analyzed by immunoblotting, as indicated. The $K^{866}R^{867}R^{868}$/AAA mutation reduced the association of CA-CaMKIIα with HA-$mGlu_5$. Data are plotted as the mean ± S.E.M. ($P = 0.028$, one sample t test; $n = 4$). p-Thr286, phospho-Thr286. In the bar graphs for both panels, * indicates $P<0.05$.

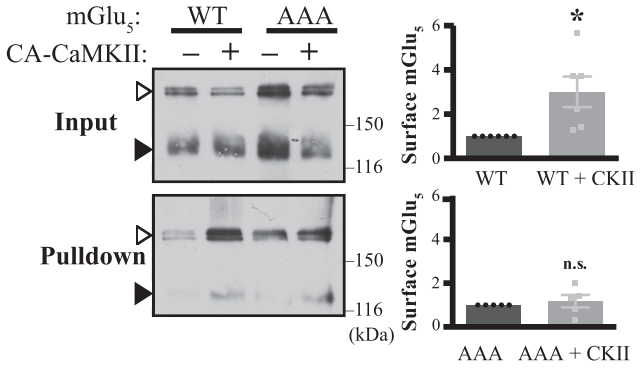

Fig. 5. CaMKII enhances the cell-surface expression of $mGlu_{5a}$ via interaction with the CTD. Cell-surface biotinylation analyses of HEK293A cells expressing $mGlu_{5a}$ (WT or with $K^{866}R^{867}R^{868}$/AAA mutation in the CTD) with either mApple or mApple-tagged CA-CaMKIIα. The coexpression of CA-CaMKIIα increased steady-state surface expression levels of WT $mGlu_{5a}$ ($P = 0.036$, one-sample t test; $n = 6$), but not of the $K^{866}R^{867}R^{868}$/AAA mutant. Data are plotted as the mean ± S.E.M. ($P = 0.569$, one-sample t test; $n = 5$). *$P<0.05$; n.s., non-significant.

sample t test vs. hypothetical value of 1) (Fig. 5). To determine whether CaMKIIα interaction with the $mGlu_{5a}$-CTD is important for this effect, we examined the cell-surface expression of $mGlu_{5a}$-AAA. In the absence of coexpressed CaMKII, the surface expression of $mGlu_{5a}$-AAA was not significantly different from those of WT $mGlu_{5a}$ [1.6 ± 0.6-fold (S.E.M.); $n = 5$; $P = 0.35$; one-sample t test vs. hypothetical value of 1]. Moreover, the coexpression of mApple-CA-CaMKIIα had no effect on cell-surface expression of $mGlu_{5a}$-AAA. These data demonstrate that interaction with the $mGlu_{5a}$-CTD is necessary for CaMKIIα-mediated increases in $mGlu_{5a}$ cell-surface expression.

CaMKIIα Reduces $mGlu_{5a}$-Stimulated Peak Ca^{2+} Mobilization. To investigate the effect of CaMKIIα on $mGlu_{5a}$ signaling, we measured glutamate-induced Ca^{2+} mobilization in populations of 293A-$5a^{LOW}$ cells that stably express $mGlu_{5a}$ and were transiently transfected to coexpress mApple or mApple-tagged CaMKIIα (either WT or CA). A similar fraction of the total cells expressed detectable levels of mApple-tagged WT- or CA-CaMKIIα in each transfection (typically ~60%). After loading glutamate-starved cells with Fluo-4-AM, a fluorescent Ca^{2+} indicator, we measured fluorescence responses of total cell populations to increasing glutamate concentrations (0.01–100 μM) (Fig. 6A). An overlay of raw traces from cells expressing mApple, mApple-WT-CaMKIIα, or mApple-CA-CaMKIIα in a representative experiment is shown in Fig. 6B. Peak Ca^{2+} responses (increased fluorescence) at each glutamate concentration were expressed as a ratio to the maximum response to a saturating concentration of glutamate (100 μM) in mApple-expressing control cells for each individual experiment, and then data were averaged across five independent experiments. Glutamate increased the peak fluorescence in a concentration-dependent manner, with an apparent EC_{50} value of 0.38 ± 0.03 μM in control cells, similar to previous analyses (Schoepp et al., 1999; Hammond et al., 2010). The glutamate response was unaffected by the coexpression of mApple-WT-CaMKIIα, but the coexpression of mApple-CA-CaMKIIα reduced peak Ca^{2+} responses at the highest concentrations of glutamate by approximately 20%, without affecting the apparent EC_{50} value (Fig. 6C). As an alternative measure of Ca^{2+} responses, we determined the area under the curve of the initial Ca^{2+} peak at the highest glutamate concentration. There was no difference in the area under the curve between cells expressing mApple or mApple-CaMKIIα-WT, but the coexpression of mApple-CA-CaMKIIα significantly reduced the area under the curve (control, 109.2 ± 2.7; WT, 101.3 ± 7.4; CA, 82.6 ± 4.1; one-way analysis of variance (ANOVA), $P = 0.011$, $F = 6.280$; Sidak's post hoc test for multiplicity–adjusted P values: WT vs. control, $P = 0.51$; CA vs. control, $P = 0.0073$) (data not shown). Since mApple-CA-CaMKIIα is expressed in only a fraction of the cell population in each well, the measured reductions in maximal Ca^{2+} responses presumably underestimate the actual impact of expressing CA-CaMKIIα in each cell. However, these data cannot differentiate whether this effect reflects decreased Ca^{2+} mobilization within each cell or a decrease in the fraction of responsive cells. Nevertheless, the data indicate that the coexpression of CA-CaMKIIα, but not WT-CaMKIIα, can reduce $mGlu_{5a}$-stimulated peak Ca^{2+} mobilization.

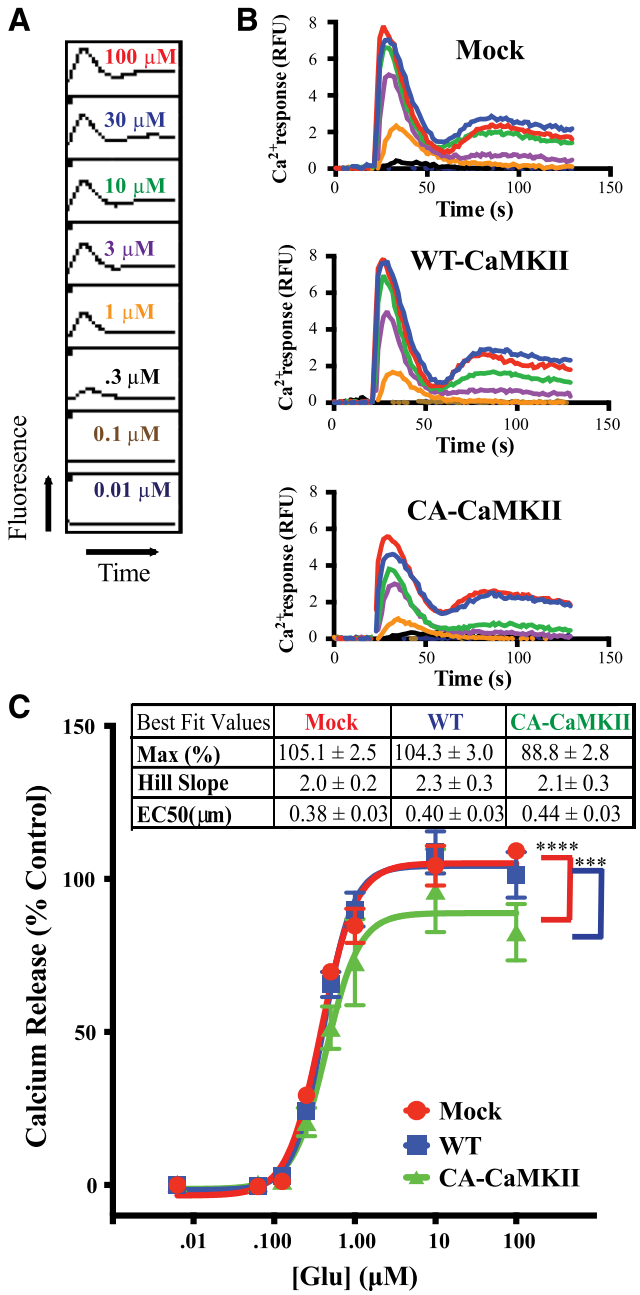

Fig. 6. CaMKIIα regulates mGlu$_{5a}$-stimulated Ca^{2+} mobilization in 293A-5a^{LOW} cells. Time courses of intracellular Ca^{2+} responses to glutamate were measured by changes in Fluo-4 fluorescence in stable 293A-5a^{LOW} cells in 96-well plates. (A) Time courses of Ca^{2+} responses. Example of calcium responses to increasing glutamate concentrations was collected in a row of eight wells. (B) Overlay of individual Ca^{2+} responses to increasing concentrations of glutamate [labeled by colors in (A)] from 293A-5a^{LOW} cells transiently transfected to express mApple control, mApple-CaMKIIα-WT, or mApple-CA-CaMKIIα from a representative experiment. (C) Concentration-response curves. Initial peak Ca^{2+} responses (ΔF/F0) at each concentration were normalized to the maximal glutamate-stimulated response in control (mApple-transfected) cells within each experiment. Normalized Ca^{2+} responses are plotted as the mean ± S.E.M. (n = 5 experiments) as a function of glutamate concentration. The expression of CaMKIIα-WT had no impact on the Ca^{2+} response curve, but the expression of CA-CaMKIIα reduced peak Ca^{2+} responses (multiple-comparisons two-way ANOVA: sources of variation: CaMKII, $P < 0.0001$; interaction, $P = 0.029$. Tukey's post hoc test for multiplicity–adjusted P values: mApple vs. WT, $P = 0.926$; mApple vs. CA-CaMKIIα, $P < 0.0001$; WT vs. CA-CaMKIIα, $P = 0.0002$). The inset table shows the maximum response (Max), EC_{50} (μM), and Hill coefficient (±S.E.M.) obtained by fitting the data in GraphPad Prism. In panel C, *** and **** indicate P<0.001 and 0.0001, respectively.

CaMKIIα Prolongs mGlu$_{5a}$-Mediated Ca^{2+} Signaling. To address caveats associated with studies investigating the effects of mApple-CA-CaMKIIα on Ca^{2+} mobilization in 293A-5a^{LOW} cells, we also examined Ca^{2+} mobilization in single HEK293A cells transfected to express full-length mGlu$_{5a}$ with either mApple alone (control) or mApple-CA-CaMKIIα. After loading all cells with Fura-2/AM, a ratiometric Ca^{2+} indicator, single cells were selected for analysis based on the presence of mApple as a marker of transfection. Application of 100 μM glutamate to cells coexpressing soluble mApple or mApple-CA-CaMKIIα with WT mGlu$_{5a}$ produced an initial peak of Fura-2 fluorescence followed by highly variable changes of fluorescence over the next 10 minutes (Fig. 7A). In a majority of cells in each group (53%–68%) Ca^{2+} signals waned over time, sometimes with a secondary shoulder, but subpopulations of the cells displayed clear Ca^{2+} oscillations that either returned to baseline between oscillations (10%–21%) or were superimposed on a more sustained Ca^{2+} elevation (18%–25%) (Supplemental Fig. 1, A–C). However, the percentage of WT mGlu$_{5a}$ cells exhibiting Ca^{2+} oscillations was unaffected by the coexpression of mApple-CA-CaMKIIα (Supplemental Fig. 1D). Since it is unclear whether oscillating and nonoscillating cell responses cause different physiologic effects, we developed an approach to analyze the responses of all cells (both oscillating and nonoscillating) across five independent experiments, revealing that the initial peak fluorescence was significantly reduced (P = 0.009) in cells expressing mApple-CA-CaMKIIα versus cells expressing mApple alone (Fig. 7B), consistent with data from stably transfected cell populations (Fig. 6). Moreover, the Ca^{2+} signal was relatively prolonged in cells expressing mApple-CA-CaMKIIα versus cells expressing mApple alone, as reflected by a statistically significant increase in the half-life of the fluorescence signal (Fig. 7A, inset; Fig. 7C). We also analyzed responses in subsets of the cells within each population that exhibited at least three baseline Ca^{2+} oscillations (Supplemental Fig. 2A). There was no statistically significant difference in the total number of mGlu$_{5a}$-mediated Ca^{2+} oscillations between transfection conditions (Supplemental Fig. 2B). However, coexpression of mApple-CA-CaMKIIα reduced the relative rate of decay of peak Ca^{2+} signals in successive oscillations (Supplemental Fig. 2C). Coexpression of mApple-CA-CaMKIIα also increased the frequency of Ca^{2+} oscillations, as reflected by a reduction of the interevent intervals (Supplemental Fig. 2D). In combination, these data confirm that CaMKIIα can reduce the amplitude of initial mGlu$_{5a}$-dependent Ca^{2+} mobilization and indicate that the relative duration of Ca^{2+} signals is extended, with increases of the frequency of oscillations when they are present.

To test the hypothesis that CaMKIIα binding to the mGlu$_{5a}$-CTD is necessary for the modulation of Ca^{2+} mobilization, we examined the effect of coexpressing mApple-CA-CaMKIIα with mGlu$_{5a}$-AAA (Fig. 7D), The replacement of Lys^{866}-Arg^{867}-Arg^{868} in the CTD with alanines had little effect on glutamate-stimulated Ca^{2+} mobilization in cells expressing mApple. Moreover, the coexpression of mApple-CA-CaMKIIα with mGlu$_{5a}$-AAA had no statistically significant effect on either the initial peak (Fig. 7E) or the duration (Fig. 7F) of the glutamate-stimulated Ca^{2+} signal relative to control cells expressing mApple alone. Furthermore, the CTD mutation had no statistically significant effect on the responses of cells displaying baseline Ca^{2+} oscillations (Supplementary

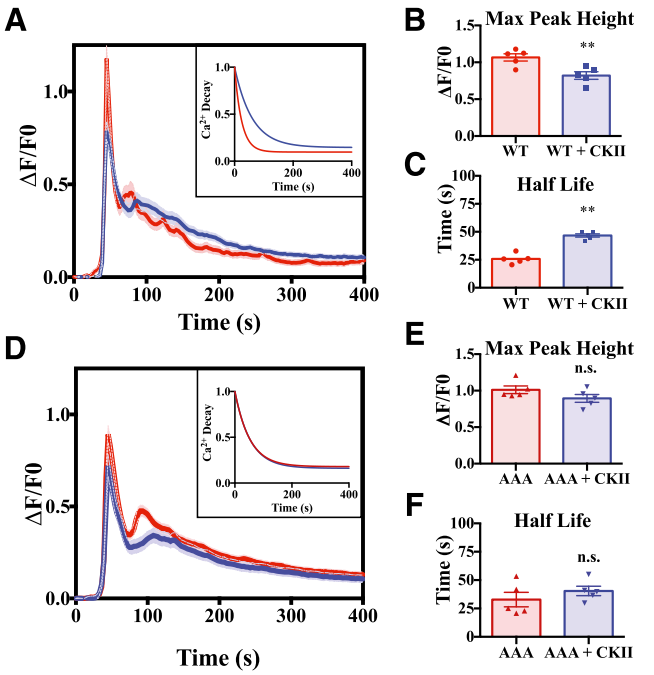

Fig. 7. CaMKIIα binding to the CTD is required for the modulation $mGlu_{5a}$-stimulated Ca^{2+} mobilization. HEK293A cells were transiently transfected to express $mGlu_{5a}$ (WT or $K^{866}RR^{868}$/AAA) with either mApple or mApple-CA-CaMKIIα for single-cell Fura-2 Ca^{2+} imaging (see *Materials and Methods*). Representative data from a single experiment. Averaged normalized changes in fluorescence from 58 to 114 cells (ΔF/F0, mean ± S.E.M.) expressing $mGlu_{5a}$-WT (A) or $mGlu_5$-$K^{866}R^{867}R^{868}$/AAA (D) in the presence (blue lines) or absence (red lines) of mApple-CA-CaMKIIα. The inset graphs show line fits for time courses of the decline of Ca^{2+} signals from the peak ΔF/F0 under each condition. (B, C, E, and F) Summary data. The bar graphs depict mean ± S.E.M. values for peak Ca^{2+} signals (ΔF/F0) (B and E) and half-lives for the decline in Ca^{2+} signals (C and F) with superimposed data points from each experiment ($n = 5$). The expression of constitutively active mApple-CA-CaMKII decreases the peak Ca^{2+} signal but increases the half-life of the Ca^{2+} signal with $mGlu_{5a}$-WT [(B) $P = 0.009$; (C) $P = 0.001$], but has no significant effect on the $mGlu_{5a}$-$K^{866}R^{867}R^{868}$/AAA mutant that disrupts CaMKII binding to the CTD [(E), $P = 0.155$; (F), $P = 0.415$]. Paired Student's t tests were used for statistical comparisons in each panel. Max, maximal. In all panels, ** indicates $P<0.01$ and n.s. indicates non-significant.

Fig. 1D) but abrogated the CaMKII-dependent modulation, as reflected by a lack of effect on the peak height decay of successive Ca^{2+} oscillations (Supplemental Fig. 2C) and the Ca^{2+} oscillation frequency (Supplemental Fig. 2D). These data indicate that binding to the $mGlu_{5a}$-CTD is important for both the increase of initial peak Ca^{2+} signals and for the prolonged Ca^{2+} signaling induced by coexpression of CA-CaMKIIα.

Discussion

In a previous report (Jin et al., 2013b), the membrane proximal region of the $mGlu_{5a}$-CTD was shown to bind inactive CaMKII. Here we extend these findings by further characterizing the physical and functional relationship between these key regulators of synaptic transmission. We confirmed that CaMKIIα and $mGlu_5$ specifically interact in mouse brain. However, our data show that $mGlu_{5a}$-CTD residues 827–964 bind more strongly to CaMKIIα in an active, Thr286-autophosphorylated conformation, but that this interaction is disrupted by excess Ca^{2+}/CaM or by robust CaMKII autophosphorylation at additional undefined sites. Furthermore, our data indicate that CaMKII binding to the CTD exerts complex effects on $mGlu_{5a}$ surface expression and downstream Ca^{2+} mobilization.

There is a growing appreciation that specific physiologic actions of CaMKII are modulated in part through dynamically regulated interactions with CaMKII-associated proteins (CaMKAPs). Several CaMKAPs preferentially interact with activated conformations of CaMKII; these CaMKAPs can be subclassified based on differences between the amino acid sequences of their CaMKII-binding domains. CaMKII-binding domains in the *N*-methyl-D-aspartate receptor GluN2B subunits and calcium channel β1 and β2 subunits resemble the CaMKII regulatory domain (Strack et al., 2000; Grueter et al., 2008). In contrast, the amino acid sequence of a CaMKII-binding domain in densin has similarity with a naturally occurring CaMKII inhibitor protein (Jiao et al., 2011). Here, we show here that the binding domain for activated CaMKII in the $mGlu_{5a}$-CTD does not resemble these CaMKAPs. Rather, this novel interaction requires three basic residues (Lys^{866}-Arg^{867}-Arg^{868}), similar to the recently identified interaction of activated CaMKII with the N-terminal domains of L-type voltage-gated Ca^{2+} channels (Wang et al., 2017). Interestingly, triple basic residue motifs can also be identified in CaMKII-binding domains of other G protein–coupled receptors, including intracellular loops of the $G\alpha_i$-coupled D_2R and D_3R (Liu et al., 2009; Zhang et al., 2014) and the CTD of the $mGlu_1$ receptor (Jin et al., 2013a,b), which also couples to $G\alpha_{q/11}$ (Fig. 3). Thus, it will be interesting to investigate the role of these triple basic residue motifs in CaMKII binding to additional G protein–coupled receptors.

One unusual aspect of CaMKII binding to the $mGlu_{5a}$-CTD is that, whereas the in vitro interaction requires CaMKIIα activation and Thr286 autophosphorylation, additional autophosphorylation at non-Thr286 sites after incubation at 30°C reduces the binding. Our recent proteomics analyses of purified CaMKIIα autophosphorylated in vitro using a similar 30°C protocol detected 17 autophosphorylation sites, in addition to Thr-286 (Baucum et al., 2015). Presumably, the autophosphorylation at one or more of these non-Thr286 sites interferes with in vitro CaMKIIα binding to $mGlu_{5a}$. Although this is a potentially interesting finding, parallel proteomics analyses of CaMKII isolated from mouse brain failed to detect phosphorylation at many of these in vitro sites (Baucum et al., 2015). However, it is possible that this observation explains why Jin et al. (2013b) found that autophosphorylated CaMKII did not bind to $mGlu_{5a}$ in vitro because their autophosphorylation reactions were incubated at 30°C.

Our data show that CaMKIIα activation enhances the association with full-length $mGlu_{5a}$, and that this interaction involves the Lys^{866}-Arg^{867}-Arg^{868} motif in the CTD (Fig. 3). However, triple alanine substitution of CTD residues 866–868 reduced the interaction by only ~50%, suggesting that CaMKII may interact with additional regions in $mGlu_{5a}$ or bind to the receptor through an indirect interaction. Indeed, a CaMKII interaction with the second intracellular loop of $mGlu_5$ has been reported previously (Raka et al., 2015), although we have been unable to detect direct binding of purified CaMKII to a GST fusion protein containing the $mGlu_5$ second intracellular loop (data not shown). Although our data cannot preclude a role for a secondary or indirect interaction, our analyses in heterologous cells indicate that CaMKIIα interaction with the CTD is critical for several novel functional effects of CaMKII on $mGlu_{5a}$

signaling. First, we show here that CaMKIIα can increase cell-surface expression of $mGlu_{5a}$. Second, we found that CaMKIIα has complex effects on $mGlu_{5a}$-dependent Ca^{2+} mobilization. As noted previously, $mGlu_5$ activation can induce temporally diverse intracellular Ca^{2+} responses in heterologous cells and in neurons (Flint et al., 1999; Mao and Wang, 2003; Kim et al., 2005; Uematsu et al., 2015; Jong and O'Malley, 2017). The coexpression of CaMKII had little effect on the proportion of cells exhibiting different oscillatory or nonoscillatory response patterns (Supplementary Fig. 1). However, we found that the coexpression of CA-CaMKIIα reduces the amplitude of the initial peak Ca^{2+} signals (Fig. 6C; Fig. 7B) but prolongs the duration of the Ca^{2+} signals (Fig. 7C; Supplementary Fig. 2C) in either the total responding cell population or only in cells that exhibit baseline Ca^{2+} oscillations. The coexpression of CA-CaMKIIα also increases the frequency of baseline Ca^{2+} oscillations (Supplementary Fig. 2D). All of these effects are prevented by the triple alanine substitution for Lys^{866}-Arg^{867}-Arg^{868} in the CTD (Fig. 7, D–F; Supplementary Fig. 2, C and D). Presumably, the effect of CaMKIIα to increase basal cell-surface expression contributes to the prolongation of Ca^{2+} signaling, but the mechanisms underlying the reduced initial peak Ca^{2+} signal, observed in both stable 293A-$5a^{LOW}$ cell populations and in single transiently transfected cells, remains unclear. Taken together, our data show that binding of CaMKIIα can play an important role in modulating cellular responses to $mGlu_{5a}$ activation. Further examination into the contribution of these mechanisms in synaptic plasticity and neuronal Ca^{2+} signaling are warranted in future studies.

Interestingly, cell-surface expression of $mGlu_{5a}$ is also modulated by direct binding of Ca^{2+}/CaM to the CTD, similar to the effects of CaMKIIα binding to the CTD reported herein, and Ca^{2+}/CaM also prolongs $mGlu_5$-mediated Ca^{2+} signaling (Lee et al., 2008). The Ca^{2+}/CaM binding domain involved in mediating these effects is located 30–40 residues C-terminal to the tribasic residue motif that is critical for CaMKII binding. Nevertheless, we found that Ca^{2+}/CaM competes for the binding of activated CaMKII to the $mGlu_{5a}$-CTD in vitro (Fig. 2C). Taken together, our data suggest an intriguing model in which the binding of CaM might confer a relatively transient Ca^{2+}-dependent modulation of $mGlu_{5a}$ surface expression and signaling, but that increased CaMKIIα autophosphorylation at Thr286 would result in sustained binding to the CTD and longer-term modulation of $mGlu_{5a}$ surface expression and Ca^{2+} mobilization. Since Thr286 autophosphorylation of CaMKII is sensitive to changes in the source, duration, or frequency of Ca^{2+} signals originating from multiple channels (Pasek et al., 2015), such as those occurring during synaptic plasticity, as well as to the regulated activities of protein phosphatases, this may provide a mechanism for cross talk with other signaling pathways.

As noted above, CaMKII has also been shown to interact with a membrane-proximal region in the CTDs of $mGlu_1$ (Jin et al., 2013a), and the CaMKII-binding domain in $mGlu_1$ contains a tri-basic residue motif, similar to the motif we have identified here as being critical for CaMKII binding to the $mGlu_{5a}$-CTD. However, CaMKII was shown to desensitize $mGlu_1$ signaling, whereas we found that CaMKII prolongs $mGlu_5$ signaling. This apparently differential modulation of $mGlu_1$ and $mGlu_5$ by CaMKII may contribute to their distinct neuronal roles (Mannaioni et al., 2001; Valenti et al., 2002; Volk et al., 2006). Interestingly, the effects of CaMKII on $mGlu_1$ signaling are mediated in part by phosphorylation at Thr871, which lies within the CaMKII-binding domain. Therefore, it will be interesting to investigate whether phosphorylation is required for the effects of CaMKII on $mGlu_5$ signaling, as well as the physical interaction demonstrated here.

The effects of CaMKIIα on $mGlu_{5a}$ must also interface with the known modulation of $mGlu_5$ signaling by other mechanisms. Prior studies have shown that several protein kinases modulate $mGlu_5$ via the CTD. For example, PKC phosphorylates Ser901 in the $mGlu_{5a}$-CTD to inhibit Ca^{2+}/CaM binding and antagonize the aforementioned modulation by Ca^{2+}/CaM (Lee et al., 2008). In addition, PKA phosphorylates Ser870 in $mGlu_{5a}$, prolonging Ca^{2+} mobilization, similar to the effects of CaMKII reported here, and enhancing ERK activation (Uematsu et al., 2015). However, it was previously reported that CaMKII reduces $mGlu_5$-stimulated ERK1/2 activation and increases agonist-induced $mGlu_5$ internalization (Raka et al., 2015). It is possible that the enhanced agonist-induced internalization in part results from the increased basal surface expression reported herein (Fig. 5). Although the mechanistic relationships between these different modes of $mGlu_5$ regulation remain to be more clearly established, the convergence of Ca^{2+}/CaM, CaMKII, PKA, and PKC actions within an ~60–amino acid region in the long CTD (345 amino acids) suggests that the actions of $mGlu_5$ are tightly controlled across different time frames, presumably fine-tuning neuronal responses such as different forms of synaptic plasticity.

Acknowledgments

We thank Hyekyung Plumley Cho for help with Flex Station experiments, and Dr. David A. Jacobson and Prasanna Dadi for providing access to equipment for the single-cell Ca^{2+} imaging and for helpful discussions. We also thank Drs. David Piston and Winship Herr for generously providing various plasmids, as detailed in the text.

Authorship Contributions

Participated in research design: Marks, Shonesy, Wang, Niswender, Colbran.

Conducted experiments: Marks.

Contributed new reagents or analytic tools: Marks, Wang, Stephenson, Niswender.

Performed data analysis: Marks, Shonesy.

Wrote or contributed to the writing of the manuscript: Marks, Shonesy, Colbran.

References

Ade KK, Wan Y, Hamann HC, O'Hare JK, Guo W, Quian A, Kumar S, Bhagat S, Rodriguiz RM, Wetsel WC, et al. (2016) Increased metabotropic glutamate receptor 5 signaling underlies obsessive-compulsive disorder-like behavioral and striatal circuit abnormalities in mice. *Biol Psychiatry* **80**:522–533.

Baucum AJ II, Shonesy BC, Rose KL, and Colbran RJ (2015) Quantitative proteomics analysis of CaMKII phosphorylation and the CaMKII interactome in the mouse forebrain. *ACS Chem Neurosci* **6**:615–631.

Cho HP, Garcia-Barrantes PM, Brogan JT, Hopkins CR, Niswender CM, Rodriguez AL, Venable DF, Morrison RD, Bubser M, Daniels JS, et al. (2014) Chemical modulation of mutant mGlu1 receptors derived from deleterious GRM1 mutations found in schizophrenics. *ACS Chem Biol* **9**:2334–2346.

Choi KY, Chung S, and Roche KW (2011) Differential binding of calmodulin to group I metabotropic glutamate receptors regulates receptor trafficking and signaling. *J Neurosci* **31**:5921–5930.

Coultrap SJ, Freund RK, O'Leary H, Sanderson JL, Roche KW, Dell'Acqua ML, and Bayer KU (2014) Autonomous CaMKII mediates both LTP and LTD using a mechanism for differential substrate site selection. *Cell Rep* **6**:431–437.

Enz R (2012) Structure of metabotropic glutamate receptor C-terminal domains in contact with interacting proteins. *Front Mol Neurosci* **5**:52.

Flint AC, Dammerman RS, and Kriegstein AR (1999) Endogenous activation of metabotropic glutamate receptors in neocortical development causes neuronal calcium oscillations. *Proc Natl Acad Sci USA* **96**:12144–12149.

Foster DJ and Conn PJ (2017) Allosteric modulation of GPCRs: new insights and potential utility for treatment of schizophrenia and other CNS disorders. *Neuron* **94**:431–446.
Giese KP, Fedorov NB, Filipkowski RK, and Silva AJ (1998) Autophosphorylation at Thr286 of the alpha calcium-calmodulin kinase II in LTP and learning. *Science* **279**:870–873.
Gregory KJ, Noetzel MJ, Rook JM, Vinson PN, Stauffer SR, Rodriguez AL, Emmitte KA, Zhou Y, Chun AC, Felts AS, et al. (2012) Investigating metabotropic glutamate receptor 5 allosteric modulator cooperativity, affinity, and agonism: enriching structure-function studies and structure-activity relationships. *Mol Pharmacol* **82**:860–875.
Grueter BA, McElligott ZA, Robison AJ, Mathews GC, and Winder DG (2008) In vivo metabotropic glutamate receptor 5 (mGluR5) antagonism prevents cocaine-induced disruption of postsynaptically maintained mGluR5-dependent long-term depression. *J Neurosci* **28**:9261–9270.
Hammond AS, Rodriguez AL, Townsend SD, Niswender CM, Gregory KJ, Lindsley CW, and Conn PJ (2010) Discovery of a novel chemical class of mGlu(5) allosteric ligands with distinct modes of pharmacology. *ACS Chem Neurosci* **1**:702–716.
Hu NW, Nicoll AJ, Zhang D, Mably AJ, O'Malley T, Purro SA, Terry C, Collinge J, Walsh DM, and Rowan MJ (2014) mGlu5 receptors and cellular prion protein mediate amyloid-β-facilitated synaptic long-term depression in vivo. *Nat Commun* **5**:3374.
Huber KM, Roder JC, and Bear MF (2001) Chemical induction of mGluR5- and protein synthesis--dependent long-term depression in hippocampal area CA1. *J Neurophysiol* **86**:321–325.
Jalan-Sakrikar N, Bartlett RK, Baucum AJ II, and Colbran RJ (2012) Substrate-selective and calcium-independent activation of CaMKII by α-actinin. *J Biol Chem* **287**:15275–15283.
Jia Z, Lu Y, Henderson J, Taverna F, Romano C, Abramow-Newerly W, Wojtowicz JM, and Roder J (1998) Selective abolition of the NMDA component of long-term potentiation in mice lacking mGluR5. *Learn Mem* **5**:331–343.
Jiao Y, Robison AJ, Bass MA, and Colbran RJ (2008) Developmentally regulated alternative splicing of densin modulates protein-protein interaction and subcellular localization. *J Neurochem* **105**:1746–1760.
Jiao Y, Jalan-Sakrikar N, Robison AJ, Baucum AJ 2nd, Bass MA, and Colbran RJ (2011) Characterization of a central Ca2+/calmodulin-dependent protein kinase IIα/β binding domain in densin that selectively modulates glutamate receptor subunit phosphorylation. *J Biol Chem* **286**:24806–24818.
Jin D-Z, Guo M-L, Xue B, Fibuch EE, Choe ES, Mao L-M, and Wang JQ (2013a) Phosphorylation and feedback regulation of metabotropic glutamate receptor 1 by calcium/calmodulin-dependent protein kinase II. *J Neurosci* **33**:3402–3412.
Jin D-Z, Guo M-L, Xue B, Mao L-M, and Wang JQ (2013b) Differential regulation of CaMKIIα interactions with mGluR5 and NMDA receptors by Ca(2+) in neurons. *J Neurochem* **127**:620–631.
Jin DZ, Xue B, Mao LM, and Wang JQ (2015) Metabotropic glutamate receptor 5 upregulates surface NMDA receptor expression in striatal neurons via CaMKII. *Brain Res* **1624**:414–423.
Joly C, Gomeza J, Brabet I, Curry K, Bockaert J, and Pin JP (1995) Molecular, functional, and pharmacological characterization of the metabotropic glutamate receptor type 5 splice variants: comparison with mGluR1. *J Neurosci* **15**:3970–3981.
Jong YI and O'Malley KL (2017) Mechanisms associated with activation of intracellular metabotropic glutamate receptor, mGluR5. *Neurochem Res* **42**:166–172.
Kim CH, Braud S, Isaac JT, and Roche KW (2005) Protein kinase C phosphorylation of the metabotropic glutamate receptor mGluR5 on Serine 839 regulates Ca2+ oscillations. *J Biol Chem* **280**:25409–25415.
Lee JH, Lee J, Choi KY, Hepp R, Lee JY, Lim MK, Chatani-Hinze M, Roche PA, Kim DG, Ahn YS, et al. (2008) Calmodulin dynamically regulates the trafficking of the metabotropic glutamate receptor mGluR5. *Proc Natl Acad Sci USA* **105**:12575–12580.
Li MZ and Elledge SJ (2012) SLIC: a method for sequence- and ligation-independent cloning. *Methods Mol Biol* **852**:51–59.
Liu XY, Mao LM, Zhang GC, Papasian CJ, Fibuch EE, Lan HX, Zhou HF, Xu M, and Wang JQ (2009) Activity-dependent modulation of limbic dopamine D3 receptors by CaMKII. *Neuron* **61**:425–438.
Lüscher C and Huber KM (2010) Group 1 mGluR-dependent synaptic long-term depression: mechanisms and implications for circuitry and disease. *Neuron* **65**:445–459.
Mannaioni G, Marino MJ, Valenti O, Traynelis SF, and Conn PJ (2001) Metabotropic glutamate receptors 1 and 5 differentially regulate CA1 pyramidal cell function. *J Neurosci* **21**:5925–5934.
Mao L and Wang JQ (2003) Metabotropic glutamate receptor 5-regulated Elk-1 phosphorylation and immediate early gene expression in striatal neurons. *J Neurochem* **85**:1006–1017.
Mao LM, Liu XY, Zhang GC, Chu XP, Fibuch EE, Wang LS, Liu Z, and Wang JQ (2008) Phosphorylation of group I metabotropic glutamate receptors (mGluR1/5) in vitro and in vivo. *Neuropharmacology* **55**:403–408.
Mao LM and Wang Q (2016) Phosphorylation of group I metabotropic glutamate receptors in drug addiction and translational research. *J Transl Neurosci (Beijing)* **1**:17–23.
McNeill RB and Colbran RJ (1995) Interaction of autophosphorylated Ca2+/calmodulin-dependent protein kinase II with neuronal cytoskeletal proteins. Characterization of binding to a 190-kDa postsynaptic density protein. *J Biol Chem* **270**:10043–10049.
Michalon A, Sidorov M, Ballard TM, Ozmen L, Spooren W, Wettstein JG, Jaeschke G, Bear MF, and Lindemann L (2012) Chronic pharmacological mGlu5 inhibition corrects fragile X in adult mice. *Neuron* **74**:49–56.
Miller SG, Patton BL, and Kennedy MB (1988) Sequences of autophosphorylation sites in neuronal type II CaM kinase that control Ca2(+)-independent activity. *Neuron* **1**:593–604.
Minakami R, Iida K, Hirakawa N, and Sugiyama H (1995) The expression of two splice variants of metabotropic glutamate receptor subtype 5 in the rat brain and neuronal cells during development. *J Neurochem* **65**:1536–1542.
Minakami R, Jinnai N, and Sugiyama H (1997) Phosphorylation and calmodulin binding of the metabotropic glutamate receptor subtype 5 (mGluR5) are antagonistic in vitro. *J Biol Chem* **272**:20291–20298.
Mockett BG, Guévremont D, Wutte M, Hulme SR, Williams JM, and Abraham WC (2011) Calcium/calmodulin-dependent protein kinase II mediates group I metabotropic glutamate receptor-dependent protein synthesis and long-term depression in rat hippocampus. *J Neurosci* **31**:7380–7391.
Mukherji S, Brickey DA, and Soderling TR (1994) Mutational analysis of secondary structure in the autoinhibitory and autophosphorylation domains of calmodulin kinase II. *J Biol Chem* **269**:20733–20738.
Niswender CM and Conn PJ (2010) Metabotropic glutamate receptors: physiology, pharmacology, and disease. *Annu Rev Pharmacol Toxicol* **50**:295–322.
Noetzel MJ, Rook JM, Vinson PN, Cho HP, Days E, Zhou Y, Rodriguez AL, Lavreysen H, Stauffer SR, Niswender CM, et al. (2012) Functional impact of allosteric agonist activity of selective positive allosteric modulators of metabotropic glutamate receptor subtype 5 in regulating central nervous system function. *Mol Pharmacol* **81**:120–133.
Oliet SH, Malenka RC, and Nicoll RA (1997) Two distinct forms of long-term depression coexist in CA1 hippocampal pyramidal cells. *Neuron* **18**:969–982.
Palmer MJ, Irving AJ, Seabrook GR, Jane DE, and Collingridge GL (1997) The group I mGlu receptor agonist DHPG induces a novel form of LTD in the CA1 region of the hippocampus. *Neuropharmacology* **36**:1517–1532.
Pasek JG, Wang X, and Colbran RJ (2015) Differential CaMKII regulation by voltage-gated calcium channels in the striatum. *Mol Cell Neurosci* **68**:234–243.
Raka F, Di Sebastiano AR, Kulhawy SC, Ribeiro FM, Godin CM, Caetano FA, Angers S, and Ferguson SS (2015) Ca(2+)/calmodulin-dependent protein kinase II interacts with group I metabotropic glutamate and facilitates receptor endocytosis and ERK1/2 signaling: role of β-amyloid. *Mol Brain* **8**:21.
Rich RC and Schulman H (1998) Substrate-directed function of calmodulin in autophosphorylation of Ca2+/calmodulin-dependent protein kinase II. *J Biol Chem* **273**:28424–28429.
Roche KW, Tu JC, Petralia RS, Xiao B, Wenthold RJ, and Worley PF (1999) Homer 1b regulates the trafficking of group I metabotropic glutamate receptors. *J Biol Chem* **274**:25953–25957.
Romano C, van den Pol AN, and O'Malley KL (1996) Enhanced early developmental expression of the metabotropic glutamate receptor mGluR5 in rat brain: protein, mRNA splice variants, and regional distribution. *J Comp Neurol* **367**:403–412.
Ronesi JA, Collins KA, Hays SA, Tsai NP, Guo W, Birnbaum SG, Hu JH, Worley PF, Gibson JR, and Huber KM (2012) Disrupted Homer scaffolds mediate abnormal mGluR5 function in a mouse model of fragile X syndrome. *Nat Neurosci* **15**:431–440, S1.
Saito H, Kimura M, Inanobe A, Ohe T, and Kurachi Y (2002) An N-terminal sequence specific for a novel Homer1 isoform controls trafficking of group I metabotropic glutamate receptor in mammalian cells. *Biochem Biophys Res Commun* **296**:523–529.
Schoepp DD, Jane DE, and Monn JA (1999) Pharmacological agents acting at subtypes of metabotropic glutamate receptors. *Neuropharmacology* **38**:1431–1476.
Shonesy BC, Jalan-Sakrikar N, Cavener VS, and Colbran RJ (2014) CaMKII: a molecular substrate for synaptic plasticity and memory. *Prog Mol Biol Transl Sci* **122**:61–87.
Silva AJ, Paylor R, Wehner JM, and Tonegawa S (1992a) Impaired spatial learning in alpha-calcium-calmodulin kinase II mutant mice. *Science* **257**:206–211.
Silva AJ, Stevens CF, Tonegawa S, and Wang Y (1992b) Deficient hippocampal long-term potentiation in alpha-calcium-calmodulin kinase II mutant mice. *Science* **257**:201–206.
Simonyi A, Schachtman TR, and Christoffersen GR (2005) The role of metabotropic glutamate receptor 5 in learning and memory processes. *Drug News Perspect* **18**:353–361.
Stephenson JR, Wang X, Perfitt TL, Parrish WP, Shonesy BC, Marks CR, Mortlock DP, Nakagawa T, Sutcliffe JS, and Colbran RJ (2017) A novel human *CAMK2A* mutation disrupts dendritic morphology and synaptic transmission, and causes ASD-related behaviors. *J Neurosci* **37**:2216–2233.
Strack S, McNeill RB, and Colbran RJ (2000) Mechanism and regulation of calcium/calmodulin-dependent protein kinase II targeting to the NR2B subunit of the N-methyl-D-aspartate receptor. *J Biol Chem* **275**:23798–23806.
Uematsu K, Heiman M, Zelenina M, Padovan J, Chait BT, Aperia A, Nishi A, and Greengard P (2015) Protein kinase A directly phosphorylates metabotropic glutamate receptor 5 to modulate its function. *J Neurochem* **132**:677–686.
Valenti O, Conn PJ, and Marino MJ (2002) Distinct physiological roles of the Gq-coupled metabotropic glutamate receptors Co-expressed in the same neuronal populations. *J Cell Physiol* **191**:125–137.
Volk LJ, Daly CA, and Huber KM (2006) Differential roles for group 1 mGluR subtypes in induction and expression of chemically induced hippocampal long-term depression. *J Neurophysiol* **95**:2427–2438.
Wang X, Marks CR, Perfitt TL, Nakagawa T, Lee A, Jacobson DA, and Colbran RJ (2017) A novel mechanism for Ca^{2+}/calmodulin-dependent protein kinase II targeting to L-type Ca^{2+} channels that initiates long-range signaling to the nucleus. *J Biol Chem* **292**:17324–17336.
Yang E and Schulman H (1999) Structural examination of autoregulation of multifunctional calcium/calmodulin-dependent protein kinase II. *J Biol Chem* **274**:26199–26208.
Zhang S, Xie C, Wang Q, and Liu Z (2014) Interactions of CaMKII with dopamine D2 receptors: roles in levodopa-induced dyskinesia in 6-hydroxydopamine lesioned Parkinson's rats. *Sci Rep* **4**:6811.
Zhou Y, Takahashi E, Li W, Halt A, Wiltgen B, Ehninger D, Li GD, Hell JW, Kennedy MB, and Silva AJ (2007) Interactions between the NR2B receptor and CaMKII modulate synaptic plasticity and spatial learning. *J Neurosci* **27**:13843–13853.

Address correspondence to: Dr. Roger J. Colbran, Room 702 Light Hall, Vanderbilt University School of Medicine, Nashville, TN 37232-0615. E-mail: roger.colbran@vanderbilt.edu

Supplementary Figures 1 and 2

Activated CaMKIIα binds to the $mGlu_5$ metabotropic glutamate receptor and modulates calcium mobilization

Christian R. Marks, Brian C. Shonesy, Xiaohan Wang, Jason R. Stephenson, Colleen Niswender, Roger J. Colbran

Department of Molecular Physiology and Biophysics (C.R.M., B.C.S., J.R.S., R.J.C.), Vanderbilt Brain Institute (X.W., R.J.C.), Vanderbilt Kennedy Center for Research on Human Development (C.N., R.J.C.), Department of Pharmacology (C.N.), Vanderbilt Center for Neuroscience Drug Discovery (C.N.), Vanderbilt University School of Medicine, Nashville, TN, USA

Supplemental Figure 1. Analysis of the variability of glutamate-induced $mGlu_5$ Ca^{2+} responses in transfected HEK293A cells (from data summarized in Fig. 7). Responses of individual cells could be divided into two main categories: **A**. *Non-oscillators*: An initial peak of Ca^{2+} that is sustained or returns to baseline over time (blue), in some cases with second shoulder (red), with no clear oscillations. **B**. *Oscillating cells:* The initial Ca^{2+} peak decays in an oscillatory pattern (up to ~25 oscillations in 10 min) that may (blue) or may not (red) return to baseline between successive oscillations. **C**. *Distribution of responding cells between non-oscillating or oscillating categories for each transfection condition*. The ratio of non-oscillating to oscillating HEK293A cells was not affected by co-expression of mApple-CA-CaMKIIα with WT $mGlu_{5a}$ ($p=0.28$ by Fisher's exact test) or by mutation of Lys^{866}-Arg^{867}-Arg^{868} in the CTD to alanines in $mGlu_{5a}$-AAA ($p=0.62$).

Supplementary Figure 2. Analyses of Ca^{2+} responses in baseline-oscillating HEK293A cells (blue trace in Fig. S1B) expressing $mGlu_5$-WT or $mGlu_5$-AAA with either mApple or mApple-CA-CaMKII. **A**. Overlays of ten representative Ca^{2+} responses for each transfection condition from cells selected for ≥3 baseline oscillations. **B**. There were no statistically significant differences in the total number of oscillations recorded over 10 min between transfection conditions (total numbers of baseline-oscillating cells: $mGlu_5$-WT, 78; $mGlu_5$-WT+CKII, 62; $mGlu_5$-AAA, 38; $mGlu_5$-AAA+CKII, 21. One-way ANOVA: $p = 0.08$). The error bars depict the range between the minimum (3) and maximum number of oscillations, boxes indicate the 25-75th percentile, lines within each box indicate the median, and the "+" sign within each box indicates the mean. **C**. Peak responses for the first 5 oscillations were normalized to the first Ca^{2+} peak and plotted as the mean ± SEM for each transfection condition. Co-expression of mApple-CA-CaMKII

significantly slows the rate of decay of successive peak Ca^{2+} responses in cells expressing $mGlu_{5a}$-WT, but has no effect in cells expressing $mGlu_{5a}$-AAA (2-way repeated measures ANOVA . CaMKII effect, $p<0.0001$, Sidak's test for multiplicity adjusted *p* values: $mGlu_{5a}$ vs $mGlu_{5a}$-WT+CaMKII p=0.0003, $mGlu_{5a}$ vs. $mGlu_{5a}$-AAA p>0.999, $mGlu_{5a}$-AAA vs $mGlu_{5a}$-AAA + CaMKII p>0.999). **D**. Cumulative probability curves for mean inter-event intervals in baseline-oscillating cells. Co-expression of mApple-CA-CaMKII significantly decreases inter-event intervals between Ca^{2+}-oscillations in cells expressing $mGlu_{5a}$-WT but not $mGlu_{5a}$-AAA (Kruskal Wallis test p=0.006, Dunn's test for multiplicity adjusted *p* values: WT-$mGlu_{5a}$ vs WT-$mGlu_{5a}$ + CaMKII p=0.003, WT-$mGlu_{5a}$ vs $mGlu_{5a}$-AAA p>0.999, $mGlu_{5a}$-AAA vs $mGlu_{5a}$-AAA + CKII p>0.999).

Supplemental Figure 1

A.

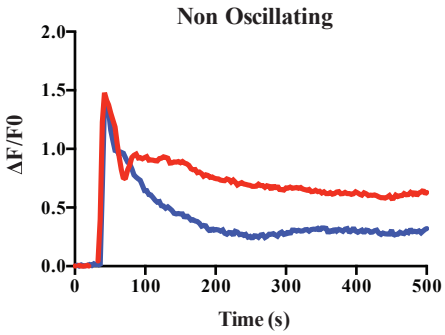

B.

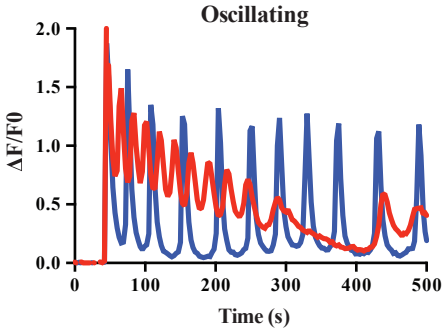

C.

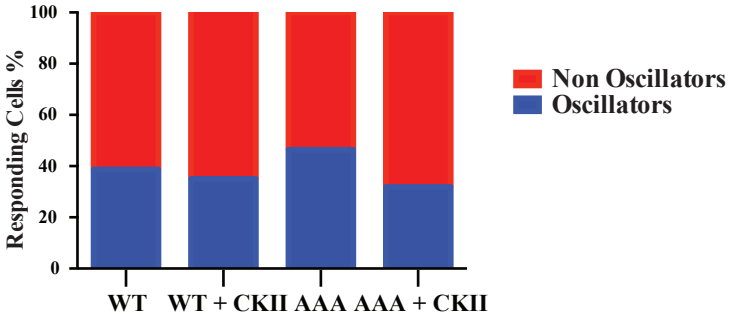

Supplemental Figure 2